REPORT

INTERFACE PHYSICS

A van der Waals interface that creates in-plane polarization and a spontaneous photovoltaic effect

Takatoshi Akamatsu[1]*, Toshiya Ideue[1]*†, Ling Zhou[2]*, Yu Dong[1], Sota Kitamura[1], Mao Yoshii[1], Dongyang Yang[3,4], Masaru Onga[1], Yuji Nakagawa[1], Kenji Watanabe[5], Takashi Taniguchi[6], Joseph Laurienzo[7], Junwei Huang[2], Ziliang Ye[3,4], Takahiro Morimoto[1], Hongtao Yuan[2], Yoshihiro Iwasa[1,8]

Van der Waals interfaces can be formed by layer stacking without regard to lattice constants or symmetries of individual building blocks. We engineered the symmetry of a van der Waals interface of tungsten selenide and black phosphorus and realized in-plane electronic polarization that led to the emergence of a spontaneous photovoltaic effect. Spontaneous photocurrent was observed along the polar direction and was absent in the direction perpendicular to it. The observed spontaneous photocurrent was explained by a quantum-mechanical shift current that reflects the geometrical and topological electronic nature of this emergent interface. The present results offer a simple guideline for symmetry engineering that is applicable to a variety of van der Waals interfaces.

Van der Waals (vdW) heterointerfaces serve as material platforms for generating exotic physical properties and functionalities and are readily fabricated with various material combinations and stacking orders (*1*–*8*). Although the symmetry of the vdW interface can be tailored, the intentional breaking of in-plane inversion symmetry and consequent functionalities are unexplored. We report the symmetry engineering of a vdW heterointerface and an experimental observation of a spontaneous quantum-mechanical shift current associated with topological electronic nature in this twisted-angle heterostructure. By stacking crystals with different rotational symmetries with a particular angle and thus reducing the interfacial symmetry, we designed a vdW interface with an in-plane electronic polarization. We observed the emergence of a controllable spontaneous photovoltaic effect (SPE)—photo-induced spontaneous current in noncentrosymmetric crystals (*9*) without a semiconductor p-n junction or bias voltage. In our system, the SPE appeared along the polar direction but was absent in the direction perpendicular to the polarization.

The SPE has attracted increasing interest not only as a new principle of photovoltaic devices but also for fundamental studies of its inherent nature and intrinsic mechanism associated with the energy band topology or geometry such as Berry curvature (dipole) or Berry connection (*10*–*15*). Investigations of the SPE in bulk polar crystals, including oxide materials (*16*–*20*), organic polar crystals (*21*), and halide compounds (*22*–*24*), and also in individual vdW bulk crystals and flakes (*25*–*28*) suggest that its emergence is closely related to symmetry reduction that creates polar symmetry. Characteristics of the SPE that we observed were also well described and understood by the polarity-induced geometrical shift current mechanism at the vdW heterointerface without commensurability.

We chose WSe_2 and black phosphorus (BP) as the building blocks of the interface because each compound has distinct rotational and mirror symmetries. WSe_2 has threefold rotational symmetry and mirror planes exist along the armchair direction, and BP has twofold rotational symmetry and sets of mirror planes (the rotational axes and mirror planes of each crystal are shown by the circled dots and green lines, respectively, in Fig. 1A). However, the heterointerface of WSe_2 and BP has no rotational symmetry because the threefold and twofold rotational symmetries are not compatible, although mirror symmetry can still remain if the mirror planes of both WSe_2 and BP are parallel. For an interface with only one mirror plane, electronic polarization would appear along the direction parallel to the mirror plane, and the resulting photocurrent generation would be expected along the in-plane polar direction.

In the WSe_2/BP interface (Fig. 1B), a stripe moiré pattern appears both along the polarization direction (parallel to the mirror plane) and vertical to the polarization direction (perpendicular to the mirror plane), unlike the hexagonal moiré patterns in twisted graphene (*7*). This stripe pattern results from the lattice mismatch between WSe_2 and BP and reflects both the trigonal symmetry of WSe_2 and the anisotropic potential of BP that

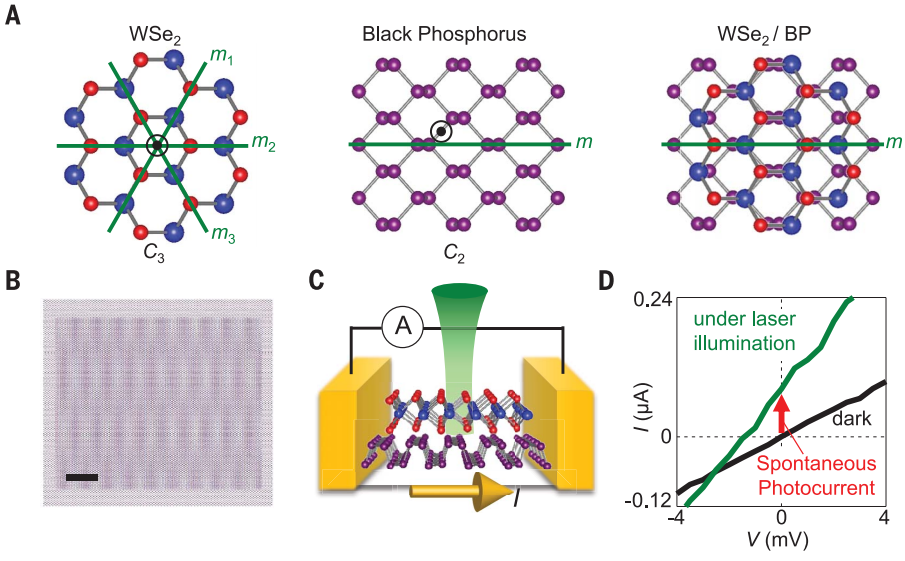

Fig. 1. Symmetry and moiré pattern of the vdW interface WSe_2/BP. (**A**) Schematic illustrations of monolayer WSe_2 (left), BP (middle), and a heterointerface of WSe_2/BP (right). Green lines and circled dots represent mirror planes and rotational axes, respectively. (**B**) Moiré patterns of the WSe_2/BP heterointerface for the case where the mirror planes of WSe_2 and BP are parallel. The scale bar (black line) represents 5 nm. (**C** and **D**) A schematic of the experiment (C) and *I*-*V* characteristic of the WSe_2/BP device (D). The spontaneous photocurrent is defined in Fig. 1D and has been measured in Figs. 2 and 3; more measurements are in the supplementary materials. The circled "A" in (C) represents the electrical system for photocurrent measurement.

[1]Quantum-Phase Electronics Center (QPEC) and Department of Applied Physics, The University of Tokyo, Tokyo 113-8656, Japan. [2]College of Engineering and Applied Sciences and National Laboratory of Solid-State Microstructures, Nanjing University, Nanjing, China. [3]Department of Physics and Astronomy, The University of British Columbia, Vancouver, BC V6T 1Z1, Canada. [4]Quantum Matter Institute, University of British Columbia, Vancouver, BC V6T 1Z4, Canada. [5]Research Center for Functional Materials, National Institute for Materials Science, 1-1 Namiki, Tsukuba 305-0044, Japan. [6]International Center for Materials Nanoarchitectonics, National Institute for Materials Science, 1-1 Namiki, Tsukuba 305-0044, Japan. [7]Department of Physics, Case Western Reserve University, Cleveland, OH, USA. [8]RIKEN Center for Emergent Matter Science (CEMS), Wako, Saitama 351-0198, Japan.
*These authors equally contributed to this work.
†Corresponding author. Email: ideue@ap.t.u-tokyo.ac.jp

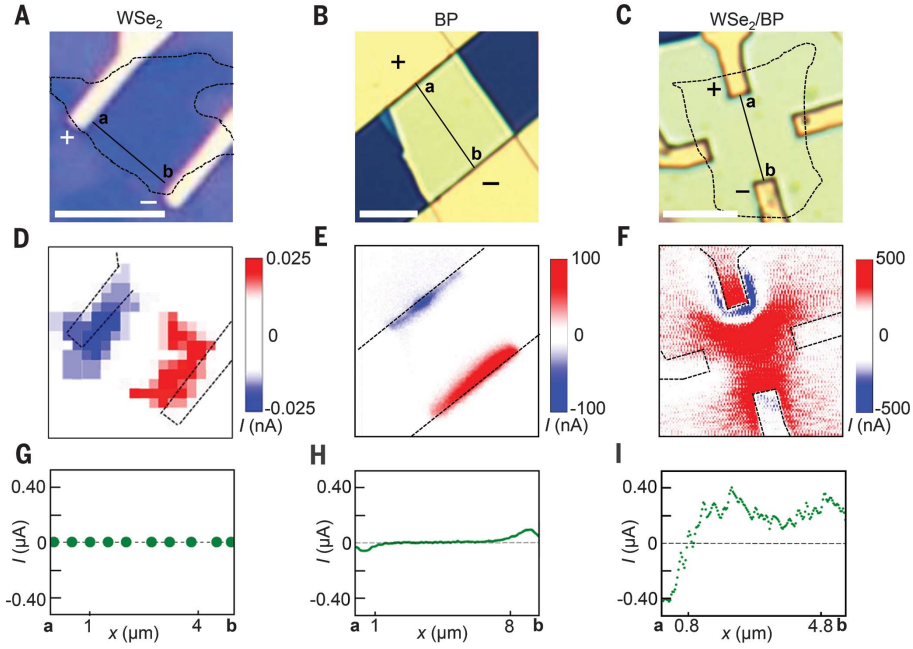

Fig. 2. Photovoltaic response in vdW crystals and interfaces with different symmetry. (**A** to **C**) Device pictures of monolayer WSe_2 (A), BP (B), and heterointerfaces of WSe_2/BP (device 1) (C). The scale bars (white lines) represent 5 μm. Dashed lines in (A) and (C) indicate the edge of monolayer WSe_2 flake, and "+" and "−" indicate the definition of the sign of the generated photocurrent. The solid black lines ab in (A) to (C) indicate the positions corresponding to the positions in (G) to (I). (**D** to **F**) Photocurrent mapping for monolayer WSe_2 (D), BP (E), and WSe_2/BP (F) devices. Linearly polarized light of 532-nm wavelength was used. The SPE emerges at the center of the WSe_2/BP interface. (**G** to **I**) Position dependence of the photocurrent along the lines in (A) to (C).

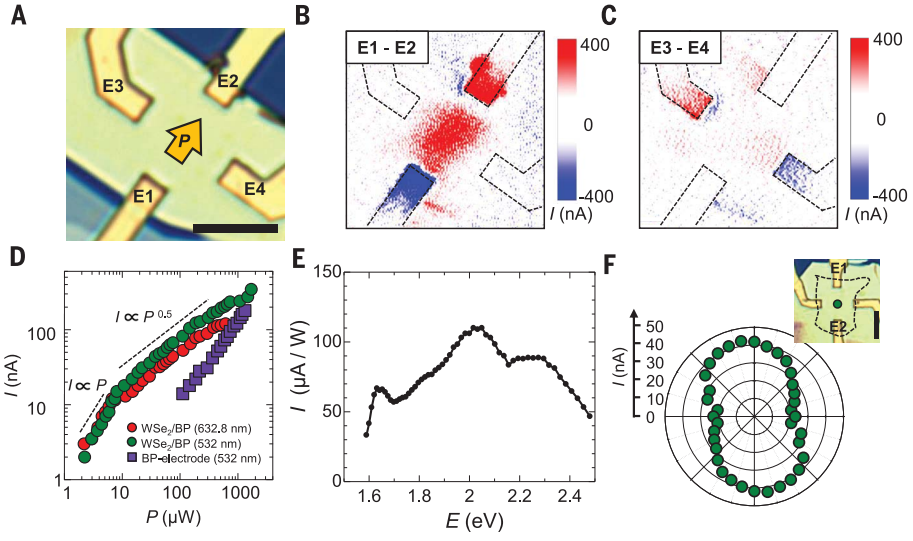

Fig. 3. Characteristics of the SPE in the WSe_2/BP interface. (**A**) Optical microscope image of the WSe_2/BP device (device 2). The scale bar (black line) represents 5 μm. (**B** and **C**) Photocurrent mapping for the E1 and E2 electrodes (B) and the E3 and E4 electrodes (C). The SPE was observed along the E1 and E2 electrode direction, whereas it is absent along the E3 and E4 electrode direction. (**D**) Laser power (P) dependence of the photocurrent (I) for two different wavelengths of 632.8 nm (red circles) and 532 nm (green circles). In the low-power region, I is proportional to P, whereas the plot shows $I \propto P^{0.5}$ power dependence in the high-power limit. On the other hand, photocurrent originating from the Schottky barrier at the electrodes of the BP device (purple squares) shows the linear power dependence. (**E**) Photon energy dependence of the photocurrent (device 2). (**F**) Polar plot of I represented by green dots as a function of the linear polarization angle along the E1 and E2 electrodes for the WSe_2/BP device (device 1). The inset shows the optical microscope image of the measured device, and the green dot within it represents the position of the laser spot.

induced the in-plane polarity at this interface. Monolayer WSe_2 transferred on BP with a thickness of around 40 to 50 nm was illuminated with a laser from the monolayer WSe_2 side (Fig. 1C; see supplementary materials for details). The room-temperature current-voltage (I-V) characteristic of the WSe_2/BP interface under dark conditions (black) or under linearly polarized light (green) is shown in Fig. 1D. A typical short circuit current under zero bias, or spontaneous photocurrent, was observed after laser illumination with a wavelength of 532 nm and intensity of 1.44 mW but not under dark conditions.

In Figure 2, we systematically studied the spatial distribution of spontaneous photocurrent in monolayer WSe_2 (Fig. 2, A, D, and G), BP (Fig. 2, B, E, and H), and the WSe_2/BP interface (Fig. 2, C, F, and I). The photocurrent mapping images (Fig. 2, D to F) were obtained by scanning the laser spot across the devices shown in Fig. 2, A to C. The SPE in the monolayer WSe_2 (Fig. 2D) and BP device (Fig. 2E) was absent when the laser illuminated the center of the devices. The generated photocurrent appeared only around the electrodes in monolayer WSe_2 and BP, which showed an antisymmetric spatial profile and could be attributed to the effect of the Schottky barriers, photothermal effects, or both (*10*, *25*, *26*).

In the WSe_2/BP stacking device, a photocurrent was observed even when the laser spots were far from the electrodes (Fig. 2F). This observation of the SPE only in the WSe_2/BP device indicated that it originated from the changes in the symmetry at the interface. The SPE appeared at the interface in several measured devices (devices 1 through 4; see supplementary materials). The SPE was also observed around the electrodes with antisymmetric spatial distribution, as shown in the position dependence of the photocurrent along the lines in Fig. 2C (Fig. 2I).

To clarify the intrinsic nature of the SPE at the WSe_2/BP interface, we measured the directional dependence of the photocurrent response. We fabricated the WSe_2/BP interface so that the mirror plane of WSe_2 was parallel to that of BP (device 2; Fig. 3A). The electrodes were patterned to be either parallel (E1 and E2) or perpendicular (E3 and E4) to the expected polar direction, and spatial maps of the spontaneous photocurrent are shown in Fig. 3, B and C, respectively. The SPE was observed only for the measurement geometry with the E1 and E2 electrodes; it was negligibly small within the background noise level for the E3 and E4 electrodes. These results indicated that the electronic polarization at the interface was almost parallel to the E1 and E2 electrodes (expected polar direction) and also excluded the possibility of the SPE originating from an extrinsic mechanism such as a randomly formed p-n like potential [such as the Dember

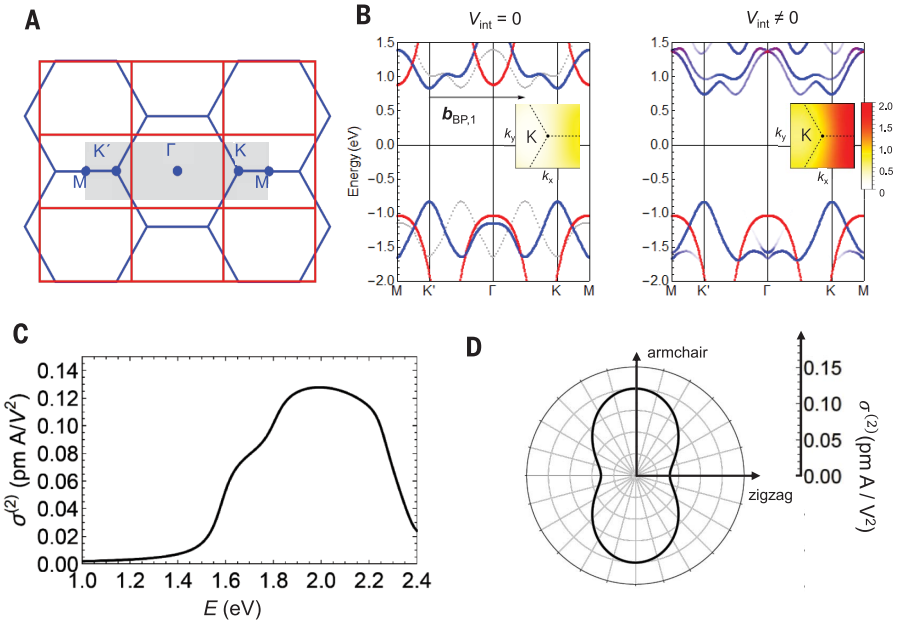

Fig. 4. Tight-binding model of the WSe_2/BP interface and its shift current. (**A**) BZs of WSe_2 (blue) and BP (red). (**B**) Energy dispersion of the tight-binding model of the WSe_2/BP interface. Interlayer coupling hybridizes the energy bands from WSe_2 and BP. The weight of the bands is color coded, with blue and red for WSe_2 and BP, respectively. The inset shows a color plot of the magnitude of the shift vector around the K point. (**C**) Nonlinear conductivity σ_{yyy} and σ_{yxx} from the shift current mechanism. (**D**) The calculated shift current along the armchair direction as a function of the linear polarization angle (E = 2.15 eV) showed no sign change and anisotropy along the polar direction.

effect (*29*)] or the anisotropy of BP. In the supplementary materials, we also present measurements of photocurrent in twisted interfaces and clarify that the direction or magnitude of the photocurrent can be tuned by stacking angle.

In Fig. 3D, we show the laser-power dependence of the spontaneous photocurrent for two different wavelengths. Both measurements show the characteristic crossover from linear to square-root dependence, an effect that could not be explained by the photovoltaic effect with Schottky barrier near the electrodes, which normally shows the linear power dependence (purple squares in Fig. 3D). Among other possible mechanisms for the SPE, the shift current mechanism, a photovoltaic effect in inversion-broken crystals that arises from the shift of the electron wave packet upon photoexcitation, is a plausible origin because it predicts such a power dependence crossover caused by a saturation of the carrier excitations (*14*).

To further understand the microscopic origin of the SPE, we studied the dependence of the bulk photovoltaic effect in the WSe_2/BP interface (device 2; Fig. 3E) with photon energy E with incident linear polarization parallel to the armchair direction. The photocurrent had peaks around E of 1.65 and 2.05 eV that seemed to correspond to the exciton peaks of WSe_2. This result indicated that exciton resonance could enhance the bulk photovoltaic response as theoretically predicted (*30*, *31*). Although the effect of excitons on the shift-current mechanism requires further investigation, these results implied that two-dimensional materials, in which excitons are stable and have a long lifetime, could enable a large photovoltaic response. In a higher-energy region (E > 2.1 eV), nonmonotonic changes were also observed (Fig. 3E).

The polar diagram of the photocurrent as a function of the linear polarization angle (Fig. 3F) showed no sign change when we rotated the polarization direction and was anisotropic along the armchair direction, which is the polar direction of the interface. This result indicated that the photocurrent was finite even if the incident light was unpolarized. The photovoltaic response is, in principle, allowed along the specific direction for the linearly polarized light in noncentrosymmetric trigonal WSe_2 (*9*), but distinct polarization angle dependence, including the sign change, was expected and photocurrent should vanish under unpolarized light in trigonal crystals. Thus, the present results cannot be explained by the bulk photovoltaic effect in trigonal crystals (in this case, the WSe_2 monolayer).

We could explain the observed photon-energy dependence in the high-energy region and polarization angle dependence with a shift current model. We used an effective tight-binding model of the WSe_2/BP interface to calculate electronic polarization (see supplementary materials) and shift current as follows: We consider tight-binding models of WSe_2 and BP layers and introduce effective coupling between the two layers. Specifically, the low-energy effective theory of the WSe_2/BP interface is described by the Hamiltonian

$$H(\boldsymbol{k}) = \begin{pmatrix} H_{WSe_2}(\boldsymbol{k}) & 0 & V_{int}(\boldsymbol{k}) \\ 0 & H_{WSe_2}(\boldsymbol{k}+\boldsymbol{b}_{BP,1}) & V_{int}(\boldsymbol{k}+\boldsymbol{b}_{BP,1}) \\ V_{int}^{\dagger}(\boldsymbol{k}) & V_{int}^{\dagger}(\boldsymbol{k}+\boldsymbol{b}_{BP,1}) & H_{BP}(\boldsymbol{k}) \end{pmatrix}$$

where H_{WSe_2} and H_{BP} are Hamiltonians for WSe_2 and BP, $\boldsymbol{k}$ is the momentum, V_{int} is the interlayer coupling, and $\boldsymbol{b}_{BP,1} \| \boldsymbol{e}_x$ is the primitive reciprocal lattice vector of BP.

This V_{int} caused the band hybridization between WSe_2 and BP that led to the spontaneous electronic polarization and the resultant shift current, as discussed below (for details, see supplementary materials). We considered the Bloch bands of WSe_2 and BP and hybridization between them at the same momentum $\boldsymbol{k}$ in the extended Brillouin zone (BZ) (Fig. 4, A and B). Although the BZ of the interface was not well defined because of the mismatch between the unit cells of WSe_2 and BP (Fig. 4A), we could still consider the Bloch bands of WSe_2 and BP and hybridization between them at the same momentum $\boldsymbol{k}$ in the extended BZ.

Once the momenta $\boldsymbol{k}$ for the two layers in the extended BZ picture were folded back into their respective first BZs, coupling appeared between Bloch states with different momenta because the two layers have different reciprocal vectors. Assuming that the interlayer coupling decayed quickly as a function of the relative position $\boldsymbol{r}$, it was sufficient to keep only a few Bloch states from each layer, which resulted in the above Hamiltonian. This treatment led to the band structure shown in Fig. 4B, where bands from WSe_2 and BP are hybridized with each other (the weight of the bands is color coded). Note that the momentum was no longer a good quantum number, and the band had a weight (less than 1) at a particular momentum $\boldsymbol{k}$ in general.

We used this model to calculate the generation of the shift current. The polarization of photoexcited electron-hole pairs was quantified by the shift vector that was defined by the difference of Berry connection between valence and conduction bands (for details, see supplementary materials). The shift vector was substantially enhanced by the interlayer coupling between WSe_2 and BP (inset of Fig. 4B), and the shift current was enhanced by the hybridization of the WSe_2 and BP bands, which can be seen in the nonlinear conductivity calculated from the formula for the shift current (Fig. 4C). In the supplementary materials, we show the detailed derivation of the coupling Hamiltonian, calculation of the shift current, and another

simpler effective two-band model by which nonvanishing polarization and photocurrent can be intuitively understood. Theoretical calculation of the electronic polarization at this interface, which only exists along the mirror planes under finite interfacial coupling, is also displayed in the supplementary materials.

The observed photon energy dependence is well reproduced by this calculation and can be understood as follows: In the low-energy region (E < 2.1 eV), optical transition between bands around K (K′) points (originally WSe_2 bands) mainly contributed to the shift current. With increasing photon energy, the shift current was initially enhanced because of the increase in the density of states. It was eventually suppressed in the higher-energy region because of the reduction of shift vector. The shift current rapidly diminished when optical transitions from the different valence band (originally BP band) were allowed, which contributed a shift current with the opposite sign that resulted in partial cancellation of the signal (see supplementary materials for details).

In the above argument, we considered the interface of 1L-WSe_2 and 1L-BP. Further calculations confirmed that the magnitude and qualitative behavior of the photon energy dependence of the shift current was almost independent of BP thickness. Also, we experimentally clarified that the photocurrent value was not affected by BP thickness, indicating that the SPE was mainly driven by the in-plane polarity at the interface and that the thick bulk part of BP did not contribute (see supplementary materials). The anisotropic polarization angle dependence of the photocurrent without sign change was also reproduced by these calculations (Fig. 4D). The concept of "symmetry engineering" and the polarity in a nonperiodic system have been established in this work.

REFERENCES AND NOTES

1. A. K. Geim, I. V. Grigorieva, *Nature* **499**, 419–425 (2013).
2. C.-H. Lee *et al*., *Nat. Nanotechnol.* **9**, 676–681 (2014).
3. L. Britnell *et al*., *Science* **335**, 947–950 (2012).
4. T. Song *et al*., *Science* **360**, 1214–1218 (2018).
5. M. Yankowitz *et al*., *Nat. Phys.* **8**, 382–386 (2012).
6. C. R. Dean *et al*., *Nature* **497**, 598–602 (2013).
7. Y. Cao *et al*., *Nature* **556**, 43–50 (2018).
8. Y. Liu *et al*., *Nat. Nanotechnol.* **13**, 828–834 (2018).
9. B. I. Sturman, V. M. Fridkin, *The Photovoltaic and Photorefractive Effects in Noncentrosymmetric Materials* (Gordon and Breach Science Publishers, 1992).
10. Q. Ma *et al*., *Nat. Phys.* **13**, 842–847 (2017).
11. S.-Y. Xu *et al*., *Nat. Phys.* **14**, 900–906 (2018).
12. G. B. Osterhoudt *et al*., *Nat. Mater.* **18**, 471–475 (2019).
13. J. Ma *et al*., *Nat. Mater.* **18**, 476–481 (2019).
14. T. Morimoto, N. Nagaosa, *Sci. Adv.* **2**, e1501524 (2016).
15. B. M. Fregoso, T. Morimoto, J. E. Moore, *Phys. Rev. B* **96**, 075421 (2017).
16. I. Grinberg *et al*., *Nature* **503**, 509–512 (2013).
17. P. S. Brody, *J. Solid State Chem.* **12**, 193–200 (1975).
18. S. Y. Yang *et al*., *Nat. Nanotechnol.* **5**, 143–147 (2010).
19. R. Nechache *et al*., *Appl. Phys. Lett.* **98**, 202902 (2011).
20. M. Nakamura *et al*., *Phys. Rev. Lett.* **116**, 156801 (2016).
21. M. Nakamura *et al*., *Nat. Commun.* **8**, 281 (2017).
22. Z. Xiao *et al*., *Nat. Mater.* **14**, 193–198 (2015).
23. Z. Sun *et al*., *Angew. Chem. Int. Ed.* **55**, 6545–6550 (2016).
24. N. Ogawa, M. Sotome, Y. Kaneko, M. Ogino, Y. Tokura, *Phys. Rev. B* **96**, 241203 (2017).
25. H. Yuan *et al*., *Nat. Nanotechnol.* **9**, 851–857 (2014).
26. Y. J. Zhang *et al*., *Nature* **570**, 349–353 (2019).
27. A. M. Cook, B. M Fregoso, F. de Juan, S. Coh, J. E. Moore, *Nat. Commun.* **8**, 14176 (2017).
28. T. Rangel *et al*., *Phys. Rev. Lett.* **119**, 067402 (2017).

ACKNOWLEDGMENTS

Funding: This work was supported by JSPS Grant-in-Aid for Scientific Research (S) (JP19H05602), the A3 Foresight Program, Grant-in-Aid for Challenging Research (Exploratory) (no. JP19K21843), Grant-in-Aid for Scientific Research on Innovative Areas (JP20H05264), Grant-in-Aid for Scientific Research (B) (JP19H01819), JST PRESTO (JPMJPR19L1 and JPMJPR19L9), JST CREST (JPMJCR19T3) and Grant-in-Aid for JSPS Fellows (JP17J08941 and JP17J09152). M.O. was supported by the Advanced Leading Graduate Course for Photon Science (ALPS). Y.N. was supported by the Materials Education program for the future leaders in Research, Industry, and Technology (MERIT) J.L. was supported by the Nakatani RIES program. H.Y. acknowledges support from the National Natural Science Foundation of China (91750101, 51861145201, 52072168, and 21733001), the National Key Basic Research Program of the Ministry of Science and Technology of China (2018YFA0306200), the Fundamental Research Funds for the Central Universities (021314380078, 021314380104, and 021314380147), the Priority Academic Program Development of Jiangsu Higher Education Institutions (021314416201), and Jiangsu Key Laboratory of Artificial Functional Materials. D.Y. and Z.Y. acknowledge support from the Natural Sciences and Engineering Research Council of Canada, Canada Foundation for Innovation, New Frontiers in Research Fund, Canada First Research Excellence Fund, and Max Planck–UBC–UTokyo Centre for Quantum Materials. Z.Y. is also supported by the Canada Research Chairs Program. **Author contributions:** T.I. and Y.I. conceived and designed the experiments. T.A. and D.Y. made and characterized devices. Y.N. developed the transfer technique. T.A., T.I., L.Z., J.H., M.O., D.Y., Y.Z., and H.Y. performed the photocurrent mapping and spectrum measurement. S.K., M.Y., and T.M. performed the theoretical analysis. T.A., T.I., H.Y., and Y.I. wrote the manuscript with input from all authors. **Competing interests:** The authors declare no competing financial interests. **Data and materials availability:** The data that support the plots within this paper and other findings of this study are available from the corresponding author upon reasonable request.

SUPPLEMENTARY MATERIALS

science.sciencemag.org/content/372/6537/68/suppl/DC1
Materials and Methods
Supplementary Text
Figs. S1 to S13
References (*29*–*39*)

19 October 2019; resubmitted 14 December 2020
Accepted 18 February 2021
10.1126/science.aaz9146

Science

A van der Waals interface that creates in-plane polarization and a spontaneous photovoltaic effect

Takatoshi Akamatsu, Toshiya Ideue, Ling Zhou, Yu Dong, Sota Kitamura, Mao Yoshii, Dongyang Yang, Masaru Onga, Yuji Nakagawa, Kenji Watanabe, Takashi Taniguchi, Joseph Laurienzo, Junwei Huang, Ziliang Ye, Takahiro Morimoto, Hongtao Yuan and Yoshihiro Iwasa

Science **372** (6537), 68-72.
DOI: 10.1126/science.aaz9146

Engineering interface polarization

Many properties can emerge at the interface of van der Waals materials created by rotating the layers of a single material or by creating heterointerfaces between different materials. Akamatsu *et al.* formed an interface that intentionally broke in-plane inversion symmetry by combining crystals of tungsten diselenide with threefold rotational symmetry and black phosphorus with twofold rotational symmetry. This interface creates in-plane electronic polarization that results in a spontaneous photovoltaic effect only along the polarization direction. This effect was explained in terms of a shift current mechanism.

Science, this issue p. 68